International Journal of Thermodynamics (IJoT)
ISSN 1301-9724 / e-ISSN 2146-1511
https://dergipark.org.tr/en/pub/ijot

Vol. 28 (No. 1), pp. 017-028, 2025
doi: 10.5541/ijot.1523093
Published online: March 1, 2025

Research Article

3E Analysis of a Hybrid Biomass / Solar System for Power Generation and Desalination

[1]* E. M. Leal, [2]E. A. Teixeira

[1] Department of Mechanical Engineering, School of Mining, Federal University of Ouro Preto, MG, Brazil.
[2] Graduate Program in Mechanical Engineering, School of Mining, Federal University of Ouro Preto, MG, Brazil.
E-mails: [1]*elisangelamleal@ufop.edu.br, edilberto.teixeira@aluno.ufop.edu.br

Received 27 July 2024, Revised 15 January 2025, Accepted 28 January 2025

Abstract

The study addresses global energy challenges by proposing a hybrid biomass and solar energy system for power generation and water desalination. A model is applied to two cities in Northeast Brazil (Natal-RN and Fortaleza-CE), targeting urban centers with waste and sunny coastal regions. Key variables include residue composition, heating value, and quantity, essential for energy efficiency assessment. Energy, exergy, and economic (3E) analyses using Scilab software compare four configurations: the base Rankine cycle, Rankine with an external superheater (ESH), Rankine with concentrated solar power (CSP), and Rankine with CSP integrated with desalination. Results show that higher pressures and temperatures enhance efficiency, reducing solar field area by 16% when pressure and temperature increase from 4.5 MPa/400°C to 6.5 MPa/500°C. Fortaleza-CE, with higher solar irradiation, requires smaller solar fields than Natal-RN. Integrating desalination into CSP cycles increases Levelized Cost of Energy (LCOE) by up to 7.6% and solar field area due to higher energy demands but provides potable water, with water recovery rates around 10% of seawater input. The findings underscore the importance of optimizing operating conditions and leveraging local solar resources to maximize socio-economic benefits.

Keywords: *Hybrid system; biomass; solar energy; power generation; desalination.*

1. Introduction

The increasing demand for energy highlights the need to implement renewable sources as safe, reliable, and economical alternatives while reducing greenhouse gas emissions and ensuring system resilience to fluctuations [1].

Renewable energy systems are categorized as single-source or hybrid systems. Single-source systems rely on one energy source, like wind or solar, supported by storage and electrical devices. Hybrid systems, however, combine two or more power generation options, integrating renewable and non-renewable sources along with storage and electrical components [2].

This paper explores renewable solutions for electricity generation and desalination in Brazil, emphasizing solar systems for fuel cost savings in regions with high solar potential. However, intermittency and battery life challenges necessitate integrating continuous energy sources such as geothermal, biomass, or ocean thermal energy [3].

Studies on thermodynamic and economic analyses of hybrid systems demonstrate their cost-effective and sustainable potential. Combined heat and power (CHP) systems improve efficiency through heat utilization for both power and heating. Advanced heat transfer strategies, including hybrid nanofluids (e.g., Al_2O_3-SiO_2/water) and magnetite nanofluids, significantly enhance convective heat transfer and reduce energy losses, showcasing innovative approaches in renewable energy systems [4], [5], [6], [7].

Table 1 highlights diverse applications of hybrid renewable energy systems that integrate solar, wind, biomass, and fuel cell technologies. These studies underline improvements in efficiency, cost reduction, carbon footprint minimization, and innovative technological approaches to address energy demands and environmental goals.

Desalination is a key focus of this research due to water scarcity, with Earth's water being 96.5% oceanic. The Humidification-Dehumidification (HDH) process is chosen for its simpler design, lower temperatures, and atmospheric pressure operation, making it a cost-effective option for decentralized applications. However, HDH has lower energy efficiency and water recovery rates compared to advanced technologies like Reverse Osmosis (RO) [28], [29].

Reverse Osmosis (RO) is the most widely used desalination method due to its efficiency and scalability, with recovery rates of 40–60%. However, its higher energy consumption (2–6 kWh/m³ for seawater) and complex pre-treatment requirements increase costs. In contrast, HDH offers lower energy demands, making it suitable for regions with solar energy and limited infrastructure [29], [30].

Alternative desalination methods include Membrane Distillation (MD), which uses low-grade heat and achieves high salt rejection rates, and Electrodialysis (ED), effective for brackish water with lower energy consumption than RO. However, MD's higher costs and ED's limitations with high-salinity water make RO the preferred choice, while HDH remains a practical solution for decentralized regions with high-salinity water [31], [32].

Wind-powered desalination systems paired with RO or ED offer renewable solutions but require energy storage due to wind

*Corresponding Author

intermittency, raising costs. HDH integrates seamlessly with solar energy, aligning with natural solar cycles, making it more cost-effective and sustainable for sun-rich, decentralized communities [33].

Biomass is highlighted as a renewable energy source capable of simultaneously producing energy, fuels, and bio-based materials. In Brazil, 81.8 million tons of municipal solid waste (MSW) were produced in 2022, with 61% disposed of in landfills. Biomass conversion to energy can be achieved via thermochemical and biochemical technologies, supporting the food-energy-water nexus [34], [35], [36].

The paper shows a novel energy, exergy, and economic (3E) approach of a hybrid biomass-solar system for electricity generation and desalination. The methodology includes literature review, technical analysis, and economic modeling to evaluate energy efficiency, heat transfer rates, and cost-effectiveness of the proposed system [37].

The study proposes a model applied to two cities in Brazil's Northeast, using Scilab software to compare hybrid and conventional cycles. Results show reduced fuel consumption and savings during peak sunlight hours. Solar integration in the desalination unit using HDH technology achieves approximately 10% efficiency, addressing energy challenges and water scarcity through innovative solutions.

2. Materials and Methods

To provide a clear overview of the study's workflow, Table 2 summarize the steps followed for the technical, exergy, and economic analyses.

2.1 Characterization of the areas

The average daily global horizontal solar irradiation in Brazil ranges from 3.5 to 6.25 kWh/m^2 per year [38]. Figure 1 illustrates a solar map of Brazil displaying the values of global horizontal irradiance (GHI).

The study focuses on two Brazilian cities, Natal-RN (5°47'42"S, 35°12'32"W) and Fortaleza-CE (3°43'06"S, 38°32'34"W), both located in the northeastern region of Brazil, as shown in Figure 1.

Both cities (Fortaleza-CE and Natal-RN) benefit from high solar irradiation, with annual Global Horizontal Irradiance (GHI) values ranging between 5.5 to 6.5 kWh/m² per day (Figure 2), making them suitable for solar energy integration. Figure 2 shows that Fortaleza consistently exhibits slightly higher GHI values compared to Natal, offering an advantage in solar energy applications [39].

Regarding municipal solid waste (MSW) amount and biogas potential, both cities generate significant amounts of MSW. Natal produces 728.58 tons per day (tpd), with an estimated lower heating value (LHV) of 7,725.7 kJ/kg, while Fortaleza generates approximately 3,750.79 tpd with an LHV of 8,297.5 kJ/kg [40]. These waste streams are rich in organic matter, plastics, and paper, as described in Table 3, which are key contributors to biogas production. The average biogas composition includes 60% methane, 30% carbon dioxide, and minor components, yielding an LHV of 30 MJ/kg [41].

Table 3 shows the average gravimetric composition of municipal solid waste in Natal-RN and Fortaleza-CE, along with the results of the LHV value, which is calculated using equation (1), according to Kumar and Samader [42].

$$LHV_w = \sum_i x_i \, LHV_i \quad (1)$$

Where: x_i is the mass fraction of the residue and LHV_i is the lower heating value of each waste type.

Table 2. Summary of this work.

Step	Description	Tools/Models	Outputs
Area Characte-rization	Identification of solar and biomass potential in selected locations (Natal-RN, Fortaleza-CE).	Solar and waste data analysis	Input parameters for energy modeling.
Techni-cal Analysis	Simulation of Rankine cycles under different configurations (base, CSP, desalination, etc.).	Scilab	System efficiency and performanc e metrics.
Exergy Analysis	Assessment of irreversibilities and second-law efficiencies for all components.	Exergy balance equations	Irreversibili ty hotspots and efficiency metrics.
Econo-mic Analysis	Calculation of Levelized Cost of Energy (LCOE) and feasibility of each configuration.	LCOE formula	Financial feasibility and cost comparison

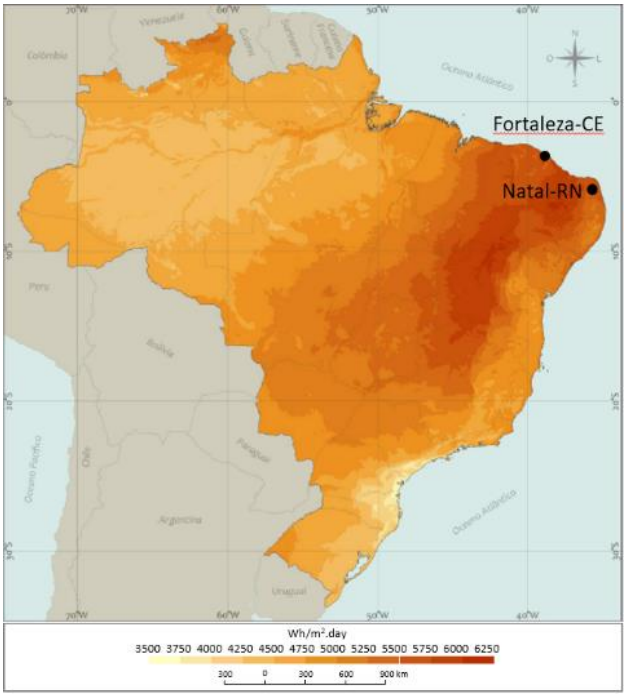

Figure 1. Annual Average Global Horizontal Irradiation in Brazil [38 adapted].

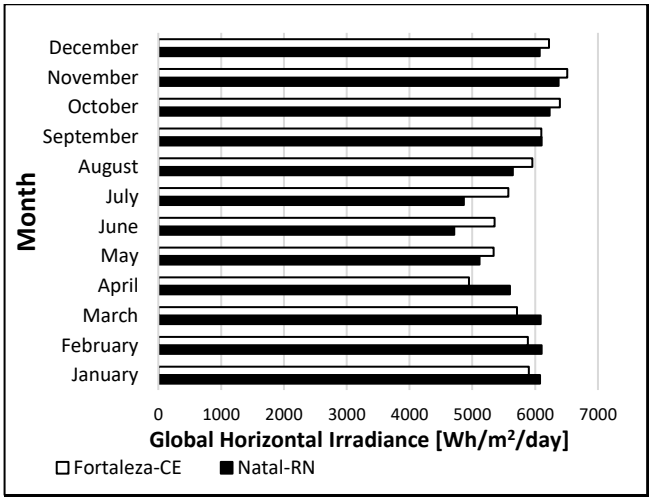

Figure 2. Monthly Average Global Horizontal Irradiation (GHI) in Natal-RN and Fortaleza-CE [39].

Table 3. Average Gravimetric Composition of MSW in Natal-RN, and Fortaleza-CE and Results of LHV.

		Natal-RN		Fortaleza-CE	
Waste Type	**LHV [kJ/kg]**	**% wt**	**LHV [kJ/kg]**	**% wt**	**LHV [kJ/kg]**
Organic Matter	5485.2	33.5	1839.74	34.9	1914.34
Paper / Cardboard	16874.1	5.2	870.70	5.9	995.57
Plastics / Tetra Pack	26363.4	17.2	4539.77	18.7	4929.95
Wood	10543.7	0.7	73.81	0.2	21.09
Textiles	14551.9	2.8	401.64	3.0	436.56
Other (recyclable)	NA	40.6	0	37.3	0
Total		**100**	**7725.7**	**100**	**8297.5**
Reference	[43]	[44 adapted]		[45 adapted]	

2.2. Base Cycle, Hybrid Cycle, and Desalination Unit

The study is based on the Rankine cycle, analyzing four configurations: (a) base Rankine cycle using municipal solid waste (MSW) as the fuel (Figure 3), (b) a Rankine cycle with an external superheater fueled by biogas from MSW (Figure 4), (c) a hybrid cycle with boiler feedwater preheating using concentrated solar power (CSP) (Figure 5), and (d) a hybrid cycle using MSW as a fuel source with CSP-based boiler water preheating and a desalination unit (Figure 6).

These cycles include the following components: (A) condensing-extraction steam turbine coupled to an electrical generator, (B) mass-burning boiler fueled by MSW, (C) condensers, (D) heat exchangers, (E) cooling tower, (F) external superheater, (G) solar field, and (P) pumps.

In the base Rankine cycle (Figure 3), the working fluid is superheated in the boiler (B), expanded in the steam turbine (A), and condensed in the condenser (C1), where it is cooled to the saturated liquid state. It then passes through the pump (P2) and the heat exchanger (D1), where it is preheated using steam extracted from the turbine. After passing through pump (P1), the fluid is pressurized before returning to the boiler (B).

In the Rankine cycle with an external superheater (Figure 4), before entering the turbine, the working fluid is superheated in an external unit powered by biogas generated from MSW. This reduces the thermal load on the boiler, protecting its components by shifting the superheating process to an external device.

In the hybrid Rankine cycle (Figure 5), the boiler feedwater (B) is preheated as it passes through a heat exchanger (D2), which receives thermal energy from the solar field (G). The fluid circulating in the solar collector is thermal oil, which indirectly transfers heat to the boiler feedwater.

In the hybrid Rankine cycle with HDH desalination (Figure 6), the solar field (G) heats saline water, which can be either seawater or brackish water. The water is initially preheated in the heat exchanger (D3) using steam from the extraction-condensing turbine (A). It is then further heated and used to humidify dry air in the humidification chamber (D4). The humidified air, now carrying steam, passes through the dehumidification chamber (C2), where it meets cooled surfaces, leading to condensation and freshwater collection, while the dry air can be recirculated.

2.3. Technical Analysis

Energy and exergy analyses of cycles are accomplished for each component or system involved. The analysis of these cycles operates under the following assumptions [37], [46]: (i) all thermodynamic processes are considered to be adiabatic (except solar collectors), and in steady state, (ii) kinetic and potential energy effects are negligible, (iii) heat loss from the pipes are negligible, (iv) at the inlet of the pumps, stream is assumed to be a saturated liquid, (v) at the inlet of the desalination process, stream from the turbine is a saturated vapor and at the outlet it is a saturated liquid, (vi) stream 14 to 15 are carried out at a constant temperature, and (vii) the water produced is pure water. The energy and exergy analyses for the cycles in Figures 3 to 6, are carried out using Scilab software and the equations provided in Table 4. Input data necessary for computational simulations are detailed in Table 5.

Table 4. Equations for the components/processes in the cycles.

Equation	
Extraction-condensing steam turbine (A) (* Rankine base / Rankine+ESH / Rankine+ESH+CSP) (**Rankine+ESH+CSP+Desal)	
$\dot{m}_{in,Turb}=\dot{m}_{out,Turb}-\sum \dot{m}_{extr,Turb}$	(2)
$n_{pol}=(h_{in}-h_{out})/(h_{in}-h_{out,s})$	(3)
$\dot{W}_{Turb}=\dot{m}_{in,Turb}(h_{in}-h_{1st\ ext})+\sum \dot{m}_{extr,Turb}\,(h_{ext}-h_{out})$	(4)
$\dot{E}x_{in,Turb}=\dot{m}_{in,Turb}ex_{in,Turb}$ (*)	(5)
$\dot{E}x_{out,Turb}=\dot{W}_{Turb}+\dot{m}_6ex_6+\dot{m}_7ex_7+\dot{E}x_{D,Turb}$ (*)	(6)
$\dot{E}x_{in,Turb}=\dot{m}_{in,Turb}ex_{in,Turb}$ (**)	(7)
$\dot{E}x_{out,Turb}=\dot{W}_{Turb}+\dot{m}_6ex_6+\dot{m}_7ex_7+\dot{m}_{14}ex_{14}+\dot{E}x_{D,Turb}$ (**)	(8)
Mass-burning Boiler (B)	
$\dot{Q}_B=\dot{m}_4(h_5-h_4)=\dot{m}_{MSW}\,LHV_{MSW}\,\eta_B+\dot{m}_{air}h_{air}$	(9)
$\dot{E}x_{in}=\dot{m}_4ex_4+\dot{m}_{MSW}\,LHV_{MSW}\,\eta_B\,\varphi_{MSW}+\dot{m}_{air}ex_{air}$	(10)
$\dot{E}x_{out}=\dot{m}_{exh}ex_{exh}+\dot{m}_5ex_5+\dot{E}x_{D,B}$	(11)
Condenser (C1)	
$\dot{Q}_{C1}=\dot{m}_6(h_6-h_1)=\dot{m}_9(h_8-h_9)$	(12)
$\dot{E}x_{in}=\dot{m}_6ex_6+\dot{m}_9\,ex_9$	(13)
$\dot{E}x_{out}=\dot{m}_1ex_1+\dot{m}_8ex_8+\dot{E}x_{D,C1}$	(14)
Dehumidifier (C2)	
$\dot{Q}_{C2}=\dot{m}_{21}h_{21}-(\dot{m}_{22}h_{22}+\dot{m}_{25}h_{25})=\dot{m}_{cw}(h_{cw,out}-h_{cw,in})$	(15)
$\dot{E}x_{in}=\dot{m}_{21}ex_{21}+\dot{m}_{cw}ex_{cw}$	(16)
$\dot{E}x_{out}=\dot{m}_{22}ex_{22}+\dot{m}_{25}ex_{25}+\dot{m}_{cw}ex_{cw}+\dot{E}x_{D,C2}$	(17)
Heat Exchanger (D1)	
$\dot{m}_2h_2+\dot{m}_7h_7=\dot{m}_3h_3$	(18)
$\dot{E}x_{in}=\dot{m}_2ex_2+\dot{m}_7ex_7$	(19)
$\dot{E}x_{out}=\dot{m}_3ex_3+\dot{E}x_{D,D1}$	(20)
Heat Exchanger (D2)	
$\dot{Q}_{D2}=\dot{m}_{11}(h_4-h_{11})=\dot{m}_{12}(h_{12}-h_{13})$	(21)
$\dot{E}x_{in}=\dot{m}_{11}ex_{11}+\dot{m}_{12}ex_{12}$	(22)
$\dot{E}x_{out}=\dot{m}_4ex_4+\dot{m}_{13}ex_{13}+\dot{E}x_{D,D2}$	(23)
Heat Exchanger (D3)	
$\dot{Q}_{D3}=\dot{m}_{14}(h_{15}-h_{14})=\dot{m}_{19}(h_{20}-h_{19})$	(24)
$\dot{E}x_{in}=\dot{m}_{19}ex_{19}+\dot{m}_{14}ex_{14}$	(25)
$\dot{E}x_{out}=\dot{m}_{15}ex_{15}+\dot{m}_{20}ex_{20}+\dot{E}x_{D,D3}$	(26)
Humidifier (D4)	
$\dot{Q}_{D4}=\dot{m}_{16}(h_{16}-h_{17})=\dot{m}_{20}h_{20}+\dot{m}_{24}h_{24}-(\dot{m}_{21}h_{21}+\dot{m}_{23}h_{23})$	(27)

Table 4. Equations for the components/processes in the cycles (continue).

Equation	
SeaWater Specific Enthalpy (h_{sw}):	
$h_{sw}=h_w-[S(27062.623+S)+S(4835.675+S).T]$	(28)
Validity [47]: h_{sw} and h_w in $\left(\frac{J}{kg}\right)$;	
10 ≤ Temp (T) ≤ 120 ºC; 0 ≤ Salinity (S) ≤ 0.12 kg/kg	
SeaWater Specific Entropy (s_{sw}) :	
$s_{sw}= s_w - S(-423.1+14630S - 98800S^2+309500$ $S^3 + 25.62T - 0.1443T^2+5.879\times10^{-4}T^3+ 80.4$ $S^2T + 0.3035\ ST^2 - 61.11\ ST)$	(29)
Validity [47]: s_{sw} and s_w in $\left(\frac{J}{kg.K}\right)$;	
10 ≤ Temp (T) ≤ 120 ºC; 0 ≤ Salinity (S) ≤ 0.12 kg/kg	
$\dot{E}x_{in}=\dot{m}_{16}ex_{16}+\dot{m}_{20}ex_{20}+\dot{m}_{24}ex_{24}$	(30)
$\dot{E}x_{out}=\dot{m}_{17}ex_{17}+\dot{m}_{21}ex_{21}+\dot{m}_{23}ex_{23}+\dot{E}x_{D,D4}$	(31)
Cooling Tower (E)	
$\dot{m}_8h_8+(\dot{m}_{air}h_{air})_{in}=\dot{m}_{10}h_{10}+(\dot{m}_{air}h_{air})_{out}$	(32)
$\dot{E}x_{in}=\dot{m}_8ex_8+\dot{m}_{air,in}ex_{air,in}$	(33)
$\dot{E}x_{out}=\dot{m}_{10}ex_{10}+\dot{m}_{air,out}ex_{air,out}+\dot{E}x_{D,E}$	(34)
Pumps (P1 / P2 / P3 / P4 / P5)	
$\dot{W}_P=\dot{m}_{in}\ v_{in}(P_{out}-P_{in})=\dot{m}_{in}\ (h_{out}-h_{in})\ \eta_P$	(35)
$\dot{E}x_{in}=\dot{m}_{in}ex_{in}+\dot{W}_P$	(36)
$\dot{E}x_{out}=\dot{m}_{out}ex_{out}+\dot{E}x_{D,P}$	(37)
External Superheater (ESH)	
$\dot{Q}_{ESH}=\dot{m}_5(h_{5b}-h_{5a})=\dot{m}_{bio}\ LHV_{bio}\ \eta_{ESH}+\dot{m}_{air}h_{air}$	(38)
$\dot{E}x_{in}=\dot{m}_5ex_{5a}+\dot{m}_{bio}\ LHV_{bio}\ \eta_{ESH}\ \varphi_{bio}+\dot{m}_{air}ex_{air}$	(39)
$Ex_{out}=\dot{m}_{exh.g}ex_{exh}+\dot{m}_5ex_{5b}+\dot{E}x_{D,ESH}$	(40)
Dehumidifier (C2)	
$\dot{Q}_{D2}=\dot{m}_{11}(h_4-h_{11})=\dot{m}_{12}(h_{12}-h_{13})$	(41)
$\dot{E}x_{in}=\dot{m}_{11}ex_{11}+\dot{m}_{12}ex_{12}$	(42)
$\dot{E}x_{out}=\dot{m}_4ex_4+\dot{m}_{13}ex_{13}+\dot{E}x_{D,D2}$	(43)
Solar Field (G)	
$\dot{Q}_{in,sun}=\eta_{col}\ I\ A_{sun}$	(44)
$A_{SF}=\dot{Q}_{col}/\left[\eta_g\ DNI\ cos(\theta)\right]$	(45)
$\dot{Q}_{HTF}=\dot{m}_{HTF}\ Cp_{HTF}\ (T_{out}-T_{in})$	(46)
System	
$\sum \dot{m}_{in} - \sum \dot{m}_{out} = 0$	(47)
$ex = ex^{ph}+ex^{ch}=[(h-h_0)-T_0(s-s_0) + \sum n_i(\mu_i-\mu_{i,0})$	(48)
Thermal Efficiency (Rankine Base - R)	
$\eta_{th,R}=\frac{\dot{W}_{Turb} - \sum \dot{W}_P - \dot{Q}_{exh}}{\dot{Q}_{MSW}}$	(49)
Thermal Efficiency (Rankine+ESH - RESH)	
$\eta_{th,RESH}=\frac{\dot{W}_{Turb} - \sum \dot{W}_P - \dot{Q}_{exh}}{\dot{Q}_{MSW} + \dot{Q}_{bio}}$	(50)
Thermal Efficiency (Rankine + CSP – RCSP):	
$\eta_{th,RCSP}=\frac{\dot{W}_T - \sum \dot{W}_P - \dot{Q}_{exh}}{\dot{Q}_{MSW} + \dot{Q}_{in,sun}}$	(51)
Thermal Efficiency (Rankine + CSP + Desal – RCSPD):	
$\eta_{th,RCSPD}=\frac{\dot{W}_T - \sum \dot{W}_P - \dot{Q}_{exh} + \dot{Q}_{D3} + \dot{Q}_{D4}}{\dot{Q}_{MSW} + \dot{Q}_{in,sun}}$	(52)

2.4. Economic Analysis

The levelized cost of energy (LCOE) is a key metric for evaluating and comparing energy generation methods. It represents the average total cost of building and maintaining an energy-producing system per unit of electricity generated over its expected lifetime [48].

LCOE is fundamental in the initial assessment of energy projects, helping determine feasibility and compare different energy ventures. It is calculated by dividing the present value of total project costs by the present value of electricity generated over the system's lifetime [49].

The significance of LCOE lies in its ability to assess project profitability. If the LCOE indicates unprofitability, companies may choose not to proceed with construction and consider alternative options. As a fundamental step in energy sector analysis, LCOE helps guide decision-making regarding investment and project viability [48]. The LCOE can be calculated using equation (53).

$$LCOE=\left[\sum_{t=1}^{n}\frac{I_t+M_t+F_t}{(1+r)^t}\right]/\left[\sum_{t=1}^{n}\frac{E_t+E_{DU}}{(1+r)^t}\right] \quad (53)$$

Where I_t are the investment costs in year t, comprising the initial price of the components, fuel handling equipment and installation cost, other equipment cost, balance of the plant and contingencies, M_t represents the operations and maintenance costs in year t, F_t are fuel costs in year t, E_t is the energy generation in year t, E_{DU} is the energy used in the desalination unit, r is the discount rate and n is the life of the system (25 years). In addition, the parameters for the economic analysis of the power plants are summarized in Table 6.

Table 5. Technical parameters of the system applied in the model.

Input Data	Unit	Natal / RN	Fortaleza/ CE
Municipal Solid Waste (MSW) Lower Heating Value (LHV)	kJ/kg	7725.7 [44]	8297.5 [45]
Biogas Lower Heating Value (LHV)	MJ/kg	10 [51]	10 [51]
Cycle Power	MW	1	1
Boiler efficiency (η_B)	%	87 [52]	87 [52]
Amb. temperature (reference state)	ºC	25 [38], [39]	25 [38], [39]
Amb. pressure (reference state)	kPa	101.325 [38], [39]	101.325 [38], [39]
Solar collector efficiency	-	0.5 [37]	0.5 [37]
Global Horiz. Irrad. (GHI)			
Higher value	Wh/m²/	6372 [38], [39]	6513 [38], [39]
Lower value	day	4712 [38], [39]	4947 [38], [39]
Boiler feed water temperature			
Without preheating	ºC	50 [52]	50 [52]
With preheating		200 [52]	200 [52]
Turbine Inlet Pressure and		4.5 MPa, 400ºC	4.5 MPa, 400ºC
Temperature (steam)	MPa, ºC	5.0 MPa, 450ºC	5.0 MPa, 450ºC
		6.5 MPa, 500ºC	6.5 MPa, 500ºC
Turbine condens. pressure	kPa	10 [53]	10 [53]
Turbine polytropic efficiency		0.85 [54]	0.85 [54]
Salt content (raw seawater)	g/kg	35 [37]	35 [37]
Seawater inlet temperature	ºC	15 [37]	15 [37]

Table 6. Parameters for the economic analysis [37],[50].

Parameter	Value
Analysis period	25 years
Site improvement	20 $/m²
Solar field	300 $/m²
Desalination unit	1500 $/m³/day
EPC and owner cost	10% of direct cost
Power plant (base)	1150 $/kWe
Power plant (base) + ESH	1200 $/kWe
Total land area	2.470 $/m²
EPC and owner cost [% direct cost]	10%
Operation and maintenance cost	55 $/kW-year

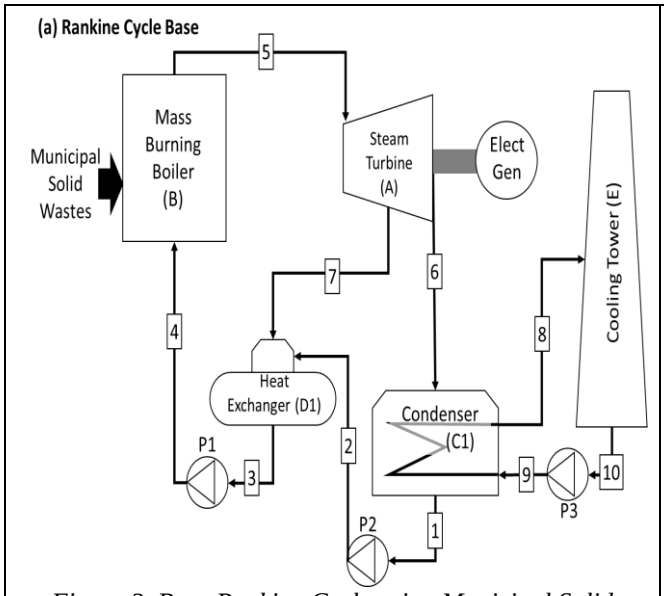

Figure 3. Base Rankine Cycle using Municipal Solid Waste (MSW) as a fuel source.

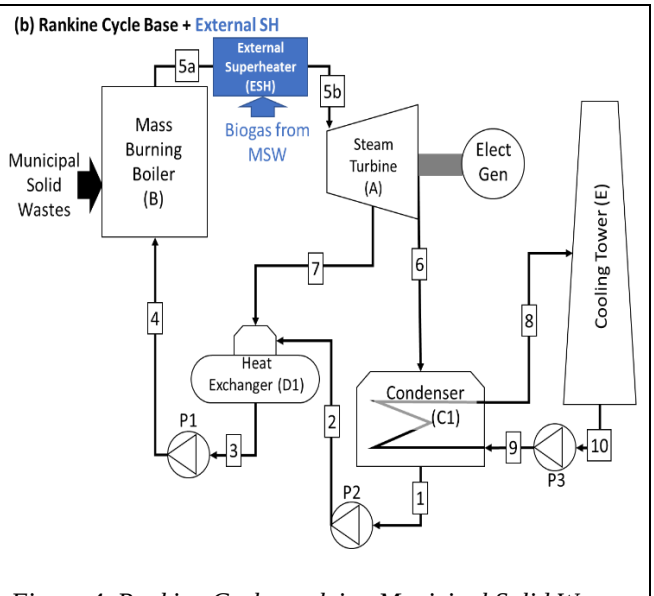

Figure 4. Rankine Cycle applying Municipal Solid Waste (MSW) as a fuel source with an external superheater fueled by biogas from MSW.

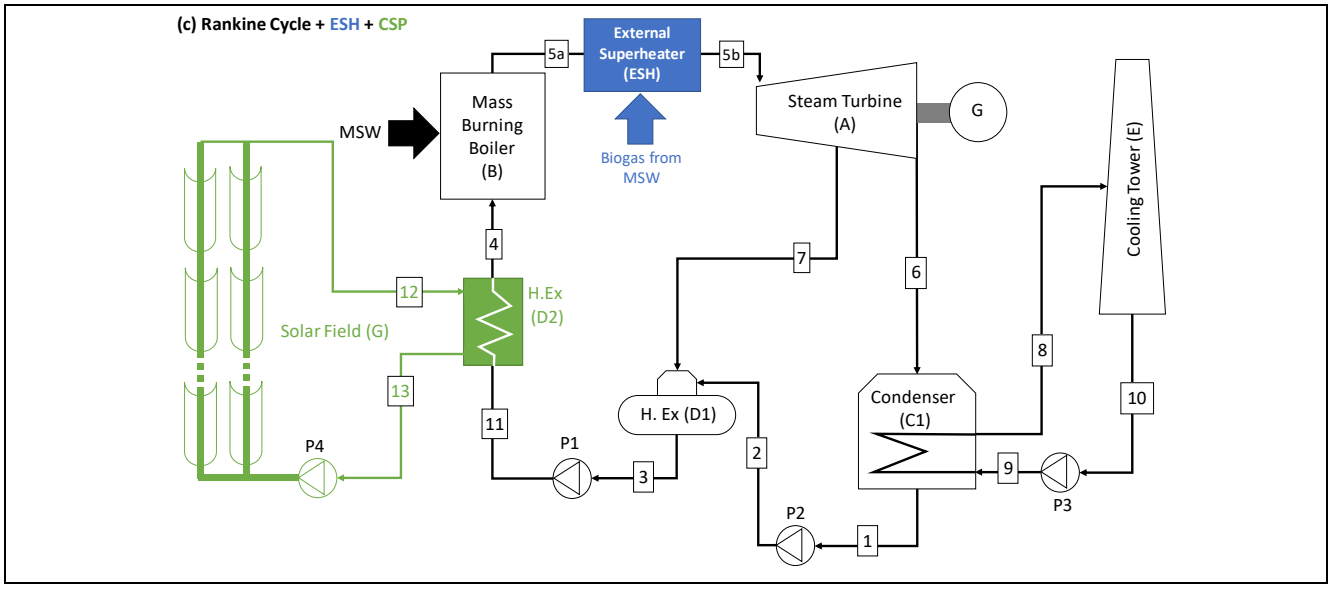

Figure 5. Hybrid Cycle using Municipal Solid Waste (MSW) as a fuel source with boiler water preheating with concentrated solar power (CSP).

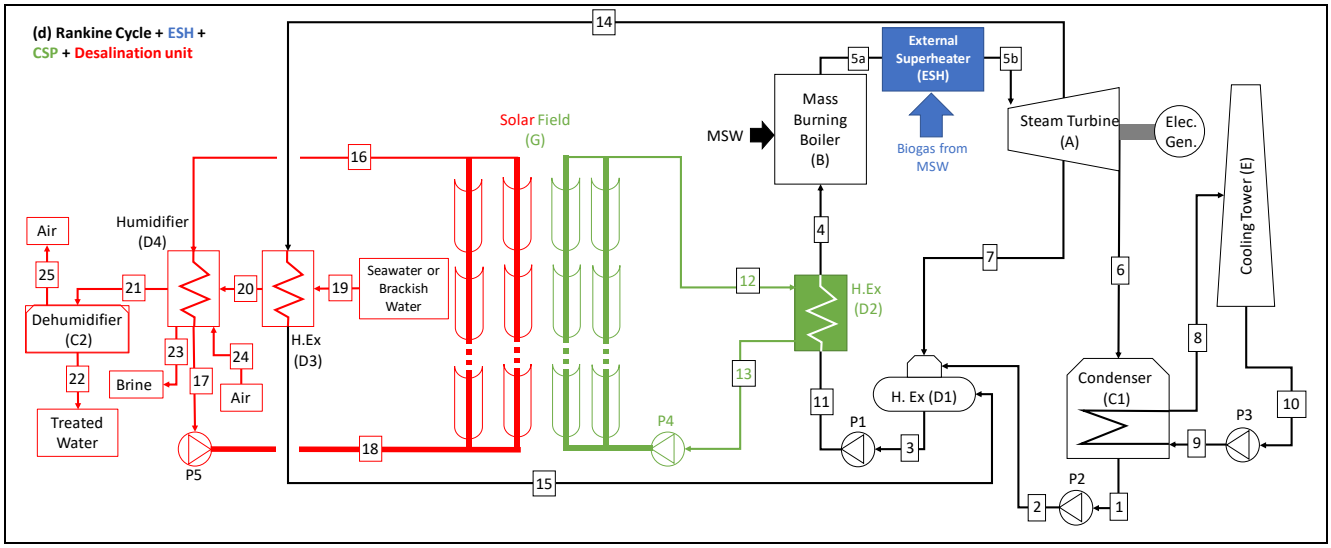

Figure 6. Hybrid Cycle using Municipal Solid Waste (MSW) as a fuel source with boiler water preheating with concentrated solar power (CSP) and a desalination unit.

2.5 Preliminary CO_2 Emission Analysis

A preliminary assessment of CO_2 emissions avoided by the hybrid biomass-solar system is conducted to evaluate its environmental benefits. The analysis considers energy contributions from the boiler and external superheater (ESH), both powered by municipal solid waste (MSW) in its raw form and as biogas. Since MSW is a renewable biomass resource, its combustion is regarded as carbon-neutral, as the CO_2 released equals the amount absorbed during biomass growth.

The avoided emissions are estimated by comparing the energy supplied by the boiler and ESH to a coal-fired power plant with an average emission factor of 0.9 kg CO_2 per kWh [55]. The methodology involves calculating the total energy produced and the corresponding CO_2 reductions achieved by substituting fossil fuels. Key assumptions include: (i) biomass energy content is based on its lower heating value (LHV), (ii) solar energy contributions are considered emission-free, and (iii) the energy consumption of auxiliary components is factored into the calculations. Equation (54) calculates the emissions avoided (E_{av}).

$$E_{av} = E_{gen} \times EF \tag{54}$$

Where: E_{gen} is the total energy generated (kWh) and EF is the emission factor for fossil fuel systems (kg CO_2 /kWh).

3. Results and Discussion

The results are divided in four sections: (i) solar concentrator, (ii) power and exergy rate, (iii) LCOE, and (iv) preliminary CO_2 emission analyses of each cycle. Figures 2 to 6, and Tables 3 to 6 are used as a base of the performed analyses.

3.1. Solar Concentrator Results

The solar concentrator model used in the analysis is a full-tracking type, with $cos(\theta)$ assumed to be 1 [50], [56]. A heat transfer fluid (HTF) is required to collect heat from the solar field. It is a synthetic thermal oil selected for its high thermal stability (up to 400°C) and low viscosity, ensuring efficient heat transfer and pumping performance. The HTF inlet and outlet temperatures are set at 250°C and 100°C, based on typical operating ranges for synthetic thermal oils in CSP systems [58]. The thermodynamic properties of the HTF follow the XCELTHERM® MK1 catalog [59], which is chemically equivalent to DOWTHERM® A and Therminol® VP-1. The solar field area, determined according to the power requirements of the CSP-integrated cycles, is showed in Table 7.

Table 7 compares different Concentrated Solar Power (CSP) cycle configurations in Natal and Fortaleza, analyzing their performance under varying Global Horizontal Irradiance (GHI) conditions. The cities exhibit different maximum and minimum GHI values, impacting CSP system efficiency.

For CSP cycles without desalination, results indicate that as pressure and temperature increase (from 4.5 MPa/400°C to 6.5 MPa/500°C), the required solar field area decreases due to improved thermodynamic efficiency. Fortaleza, with slightly higher GHI, requires a smaller solar field than Natal, demonstrating the impact of local solar insolation on field area requirements.

In CSP cycles with desalination, the solar field area is significantly larger due to the higher power demand of the desalination process. However, similar to cycles without desalination, increasing pressure and temperature reduces the required solar field area. Fortaleza, benefiting from higher GHI, requires a smaller area than Natal.

Table 7. Results of Solar Field Area based on Power Requirements for the Cycles.

Cycle	Solar Power	Natal-RN Solar Field Area		Fortaleza-CE Solar Field Area	
		(1)	(2)	(1)	(2)
Rank+ESH +CSP (4.5 MPa; 400ºC)	113.57 kW	237.6 m²	321.4 m²	232.5 m²	306.1 m²
Rank+ESH +CSP (5.0 MPa; 450ºC)	105.24 kW	220.2 m²	297.8 m²	215.4 m²	283.6 m²
Rank+ESH +CSP (6.5 MPa; 500ºC)	96.28 kW	201.5 m²	272.4 m²	197.1 m²	259.5 m²
Rank+ESH +CSP+Desal (4.5 MPa; 400ºC)	130.70 kW	273.5 m²	369.8 m²	267.6 m²	352.3 m²
Rank+ESH +CSP+Desal (5.0 MPa; 450ºC)	123.07 kW	257.5 m²	348.2 m²	251.9 m²	331.7 m²
Rank+ESH +CSP+Desal (6.5 MPa; 500ºC)	115.03 kW	240.7 m²	325.5 m²	235.5 m²	310.0 m²

(1) using maximum GHI value (2) using minimum GHI value
Rank+ESH+CSP: Rankine Cycle with an External Superheater, and Concentrated Solar Power
Rank+ESH+CSP+Desal: Rankine Cycle with an External Superheater, Concentrated Solar Power, and a Desalination unit

Power input for cycles with desalination is substantially higher, highlighting the energy-intensive nature of the process. Although efficiency improves with increased pressure and temperature, reductions in solar field area are less pronounced due to the scale of energy requirements. Both Natal and Fortaleza follow similar trends in how operating conditions influence solar field needs, while differences in solar field areas between maximum and minimum GHI values highlight the sensitivity of CSP systems to variations in solar insolation.

3.2. Power and exergy rate analyses of the cycles

Figure 7 shows the results of power, exergy rate, energy, and exergy efficiency analysis for each cycle. Figure 8 provides the exergy balance for the equipment in the hybrid system, including the desalination unit, detailing the input, output, irreversibility, and second law efficiency for each component.

Figure 7 illustrates how energy and exergy efficiencies vary with pressure, temperature, and cycle configurations. Higher efficiencies occur at 6.5 MPa and 500°C, with the best results in hybrid cycles combining ESH and CSP without desalination. The inclusion of desalination slightly decreases efficiency due to its added energy demand, but it provides the benefit of potable water production.

Net power and exergy production remain stable, peaking at 986 kW in the most efficient cycles. However, desalination cycles show lower net power output, especially at 4.5 MPa and 400°C, due to the higher energy requirements of the process.

Hybrid cycles with desalination demand higher energy and exergy inputs, but these are reduced at higher pressures and temperatures, improving energy utilization. Fortaleza-CE has a slight efficiency advantage over Natal-RN due to higher solar radiation levels, particularly in CSP-integrated cycles, where solar insolation directly impacts performance. However, both cities show similar efficiency trends, improving at higher pressures and temperatures.

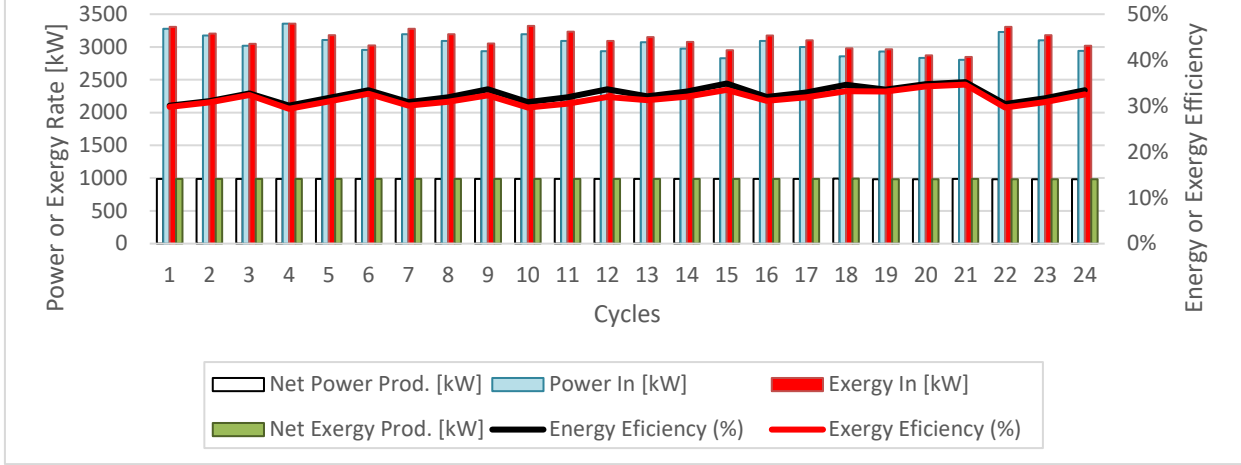

1	Rankine Base (Natal; 4.5 MPa;400ºC)	13	Rankine+ESH+CSP (Natal; 4.5MPa;400ºC)
2	Rankine Base (Natal; 5.0 MPa; 450ºC)	14	Rankine+ESH+CSP (Natal; 5.0MPa;450ºC)
3	Rankine Base (Natal; 6.5 MPa, 500ºC)	15	Rankine+ESH+CSP (Natal; 6.5MPa;500ºC)
4	Rankine Base (Fortaleza; 4.5MPa;400ºC)	16	Rankine+ESH+CSP (Fortaleza; 4.5MPa;400ºC)
5	Rankine Base (Fortaleza; 5.0MPa;450ºC)	17	Rankine+ESH+CSP (Fortaleza; 5.0MPa;450ºC)
6	Rankine Base (Fortaleza; 6.5MPa;500ºC)	18	Rankine+ESH+CSP (Fortaleza; 6.5MPa;500ºC)
7	Rankine+ESH (Natal; 4.5 MPa;400ºC)	19	Rankine+ESH+CSP+Desal (Natal; 4.5MPa;400ºC)
8	Rankine+ESH (Natal; 5.0 MPa;450ºC)	20	Rankine+ESH+CSP+Desal (Natal; 5.0MPa;450ºC)
9	Rankine+ESH (Natal; 6.5 MPa;500ºC)	21	Rankine+ESH+CSP+Desal (Natal; 6.5MPa;500ºC)
10	Rankine+ESH (Fortaleza; 4.5 MPa;400ºC)	22	Rankine+ESH+CSP+Desal (Fortaleza; 4.5MPa;400ºC)
11	Rankine+ESH (Fortaleza; 5.0 MPa;450ºC)	23	Rankine+ESH+CSP+Desal (Fortaleza; 5.0MPa;450ºC)
12	Rankine+ESH (Fortaleza; 6.5 MPa;500ºC)	24	Rankine+ESH+CSP+Desal (Fortaleza; 6.5MPa;500ºC)

Figure 7. Results of Power, Exergy Rate, Energy, and Exergy Efficiency across the analyzed cycles.

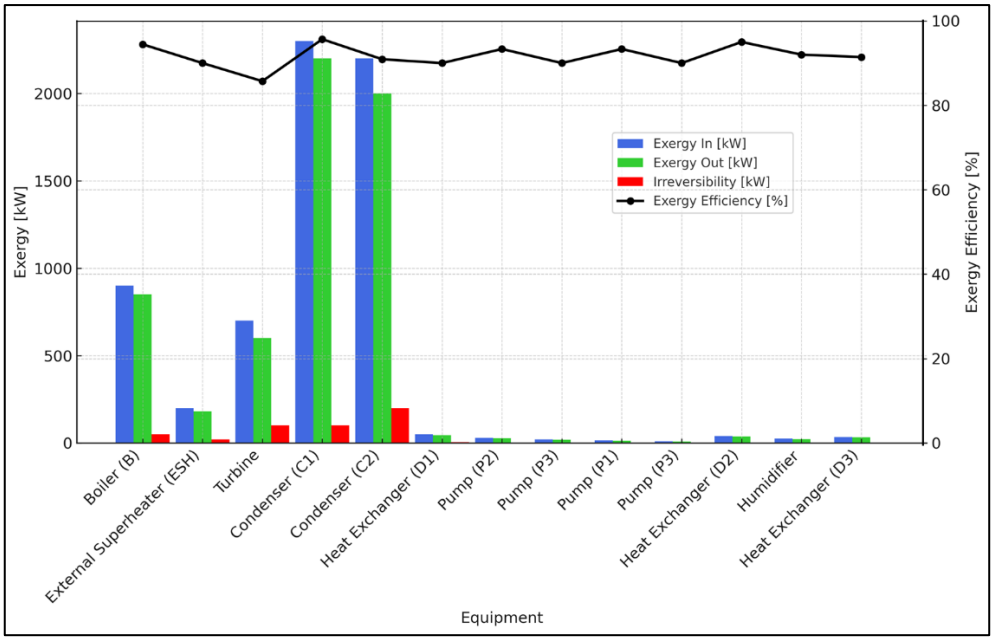

Figure 8. Results of Exergy Balance and Efficiency of the Hybrid Cycle with HDH Desalination Unit.

To enhance system performance, targeting inefficient components like the external superheater and desalination unit is decisive. Implementing advanced desalination technologies such as multi-effect distillation (MED) or reverse osmosis (RO) could reduce energy consumption and improve economic feasibility. Additionally, optimizing operating conditions and leveraging local solar potential are key to maximizing energy and exergy efficiency.

Figure 8 shows the hybrid cycle's performance, where second-law efficiency varies significantly among components. The boiler (B) has a high exergy input (~1200 kW) but operates at a low efficiency (42.7%), indicating substantial irreversibilities that could be mitigated through thermal design improvements. Similarly, the external superheater (ESH), with an exergy input of 300 kW and an efficiency of 50%, also indicates opportunities for reducing losses. In contrast, the turbine operates at 94% efficiency, effectively converting exergy into useful work, making it a key contributor to system performance. Overall, improving the boiler and ESH would enhance the system's energy utilization.

Table 8 provides a detailed thermodynamic analysis of the hybrid cycle with HDH desalination, corresponding to the pipe

numbering in Figure 6. The variations in mass flow rate, pressure, temperature, enthalpy, entropy, and exergy demonstrate the system's complexity. High-energy points (e.g., pipes 5b, 7, and 14) indicate critical energy transformation zones, where optimization could improve overall efficiency.

The desalination unit's performance (streams 19a to 25) shows that the treated water (TW, stream 22) accounts for ~10% of the total seawater input (SW, stream 19a), indicating substantial water loss. While expected due to the technology's inherent inefficiencies, this highlights the need for optimization to improve water recovery rates.

Temperature, pressure, and enthalpy variations across streams reveal heat and energy demands of the desalination process. The brine output (stream 23) retains a significant amount of energy, suggesting potential losses. The differences in entropy and exergy between input (stream 19a) and output streams (22, 23) emphasize irreversibilities in the desalination unit.

Treated water (stream 22) emerges with low exergy, indicating a simple but inefficient process. This suggests opportunities for improvement, such as alternative desalination methods or heat integration strategies to recover energy from brine (stream 23).

Table 8. Thermodynamic Properties of the Hybrid Cycle with an HDH Desalination Unit (6.5 MPa/500ºC).

Pipe number	$\dot{m}$ [kg/s]	P [kPa]	T [ºC]	h [kJ/kg]	s [kJ/kg.K]	ex [kJ/kg]
1	0.779	10	45.81	191.81	0.6492	2.80
2	0.779	1200	45.88	193.15	0.6496	4.02
3	0.998	1000	179.89	762.68	2.1384	129.67
4	0.998	6950	200	854.62	2.3223	166.78
5a	0.998	6500	300	2863.46	6.0018	1078.57
5b	0.998	6500	500	3417.12	6.8397	1382.41
6	0.793	1000	248.59	2940.1	6.9206	881.27
7	0.014	1000	248.59	2940.1	6.9206	881.27
8	25.586	195	30	125.92	0.4367	0.27
9	25.586	200	15.01	63.20	0.2245	0.82
10	25.586	100	15	63.08	0.2245	0.70
11	0.998	100	181	770.63	2.1401	137.11
12 (HTF)	0.378	150	250	738	1.0698	158.65
13 (HTF)	0.378	130	100	515	0.7272	37.79
14	0.205	1050	254.14	2950.56	6.9189	892.24
15	0.205	1000	180	2777.43	6.5856	818.48
16 (HTF)	0.107	150	250	439.8	1.3646	290.86
17 (HTF)	0.107	130	100	153.1	1.0600	91.94
18 (HTF)	0.107	200	105	523	0.7657	34.33
19a (SW)	0.100	100	15.00	63.02	0.2244	0.72
19b (SW)	0.100	200	15.04	63.16	0.2250	0.68
20 (SW)	0.100	180	21.58	90.54	0.3190	0.07
21 (Mix)	0.113	160	85.00	2299.0	1.2497	30.01
22 (TW)	0.010	100	85.00	355.90	1.1340	22.30
23 (Br)	0.090	100	85.00	373.85	1.1697	38.45
24 (Air)	0.013	100	25.00	298.60	6.8630	0.00
25 (Air)	0.013	105	85.00	359.63	7.0480	5.87

By reducing exergy losses and improving water recovery rates, the hybrid system could better integrate desalination, contributing to both energy and water sustainability.

3.3. LCOE analyses of the cycles

The Levelized Cost of Energy (LCOE) analysis is showed in Figure 9.

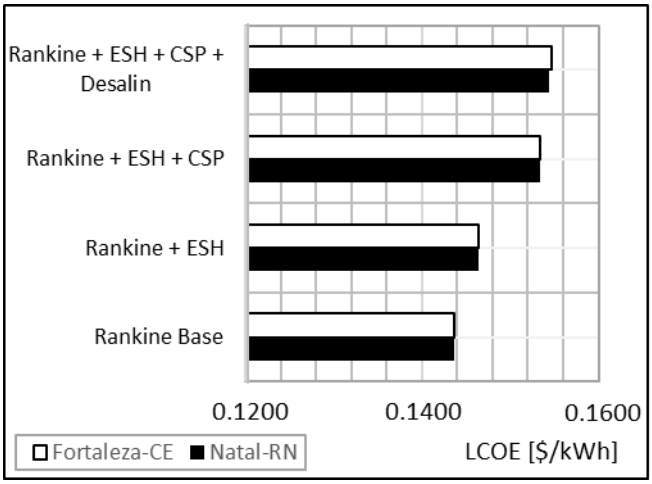

Figure 9. LCOE Comparison for Cycle Configurations in Natal and Fortaleza.

Figure 9 illustrates the Levelized Cost of Energy (LCOE) for four cycle configurations in Natal-RN and Fortaleza-CE. For the simplest cycle, Rankine Base, the LCOE is the same for both cities at 0.1436 US$/kWh. As components are added, the LCOE gradually increases. For example, in the Rank+ESH+CSP configuration, Natal shows an LCOE of 0.1533 US$/kWh, while Fortaleza is slightly higher at 0.1534 US$/kWh, a difference of 0.13%. In the most complex cycle, Rankine cycle with external superheater, concentrated solar power and a desalination unit (Rank+ESH+CSP+Desal), Natal reaches 0.1544 US$/kWh, and Fortaleza increases to 0.1546 US$/kWh, showing a 0.10% difference. These differences highlight the consistency in costs between the two cities despite local variations in solar insolation and operational conditions.

3.4. Environmental Benefits: CO_2 Emission Reductions

The results highlight the hybrid system's potential to significantly reduce CO_2 emissions by utilizing municipal solid waste (MSW) as the primary energy source for the boiler and the external superheater (ESH). By using this biomass, which would otherwise be disposed of and potentially release greenhouse gases, the system avoids emissions correlated to conventional coal-fired power plants.

For the cities studied, the avoided emissions re approximately 2561.54 kg of CO_2 per operational hour in Fortaleza-CE and 2556.05 kg of CO_2 per operational hour in Natal-RN. These values account for the energy provided by the boiler and ESH, which collectively generate 2216.99 kW and 629.16 kW in Fortaleza-CE, and 2219.50 kW and 620.56 kW in Natal-RN, respectively. The calculations assume an average emission factor of 0.9 kg CO_2eq per kWh for coal-based power plants.

This reduction demonstrates the environmental advantages of the hybrid system, as it not only influences renewable energy sources but also promotes waste valorization by converting MSW into useful energy. Future studies could expand this analysis by including emissions interrelated to the collection, transportation, and processing of MSW, offering a more comprehensive evaluation of the system's life cycle environmental impact.

4. Conclusion

The 3E analysis highlights the potential of a hybrid biomass-solar system for addressing energy and water challenges in regions with high solar potential and agricultural residues. Higher operating pressures and temperatures improve efficiency and reduce solar field area, particularly benefiting cities with higher GHI, like

Fortaleza. Integrating desalination increases energy demand and costs but provides potable water, addressing water scarcity in arid regions. Additionally, utilizing municipal solid waste and solar energy significantly reduces CO_2 emissions compared to conventional systems. Optimizing conditions can lower the LCOE, making the system feasible for areas with limited water access.

This study provides a comprehensive evaluation of hybrid systems combining biomass and solar energy, offering novel insights into energy, exergy, and economic performance. It demonstrates the feasibility of integrating desalination with CSP, addressing dual challenges of energy production and water scarcity. The research also highlights the environmental benefits of reducing CO_2 emissions through renewable energy sources and waste valorization.

Future research should explore advanced desalination technologies, such as multi-effect distillation (MED) or reverse osmosis (RO), to improve water production efficiency. Improved thermal storage materials, including molten salts or supercritical CO_2, could enhance overall system performance. Additionally, conducting comprehensive sensitivity analyses and life-cycle assessments will help refine economic and environmental sustainability, ensuring broader applicability and optimization of hybrid systems.

Statements and Declarations

The authors declare that they have no known competing financial interests or personal relationships that could have appeared to influence the work reported in this paper.

Acknowledgements

The authors would like to acknowledge the Graduate Program of Mechanical Engineering of the Federal University of Ouro Preto.

Nomenclature

A: area (m^2)
GHI: Global Horizontal Irradiation ($Wh.m^{-2}.day^{-1}$)
$\dot{E}x$: Exergy rate (kW)
$\dot{E}x_D$: Destroyed exergy rate (kW)
h: specific enthalpy ($kJ.kg^{-1}$)
LHV: lower heating value ($kJ.kg^{-1}$)
$\dot{m}$: mass flow rate ($kg.s^{-1}$)
n_{pol}: polytropic efficiency (dimensionless)
P: Pressure (kPa)
$Pol.$: Polytropic
$\dot{Q}$: heat transfer rate (kW)
s: specific entropy ($kJ.kg^{-1}.K^{-1}$)
T: temperature (K)
v: specific volume ($m^3.kg^{-1}$)
$\dot{W}$: Power (kW)
η: efficiency (dimensionless)
φ: Exergy factor (dimensionless)

Subscript

air: relative to air
amb: ambient conditions
B: boiler
bio: biogas fuel
col: solar collector
$cond$: condenser
cw: cooling water
des: destruction
$desal$: desalination unit
$extr$: extract
exh: exhaust gases
ESH: external superheater
gen: generator
HTF: heat transfer fluid (thermal oil)
$H.Ex$: heat exchanger
in: inlet
MSW: municipal solid wastes
oil: relative to the thermal oil (HTF)
out: outlet
P: pump
s: isentropic
sun: relative to the sun
SW: seawater
SF: solar field
$Turb$: turbine

Appendix

Table 1. Literature review on hybrid systems with solar / biomass and/or desalination.

Investigated System	Findings	Software used	Ref.
Concentrated solar power (CSP)-biomass hybrid plant for combined heat and power	Design and performance of a CSP-biomass plant for combined heat and power with waste heat utilization. 16.6 MW parabolic trough collector field, 10 MW biomass boilers, 4 MW ORC, 93.6% efficiency. Successful demonstration of CSP-biomass hybridization.	TRNSYS	[8]
Solar-biomass hybrid power plant in Ludhiana district, Punjab	Techno-economic feasibility analysis of solar-biomass system. Utilization of hybrid systems to overcome discontinuity in solar and wind power. Potential of the available biomass is 62.73 MW. Total connected load of the village cluster under study is 97 MW.	Homer	[9]
Hybrid solar photovoltaic-biomass gasifier system for electricity generation	Development of electric power generation system based on hybrid solar PV and biomass gasifier for rural regions of Central and South America. System includes rice and coffee husks for syngas.	Matlab	[10]
Biomass-solar on-grid hybrid power generation system for Burdur Mehmet Akif Ersoy University Istiklal Campus	Optimum system: 5000 kW photovoltaic panels, 1500 kW biomass generator, grid assistance of 3000 kW. Net present cost of USD 18.8 million, cost of energy of USD 0.107/kWh, and renewable fraction is 49.4%.	RET Screen	[11]
Biomass steam generator integrated with linear Fresnel solar field	Evaluation of biomass steam generator at partial loads integrated with solar field. Model verification using on-site measurement data. 50 t/h superheated steam at 420°C/45 bar(a), efficiency evaluation with ASME PTC4 standard.	EES (Engineering Equation Solver)	[12]
Concentrated solar power (CSP)-biomass hybrid power plants	Profitability assessment of CSP-biomass hybrid plants in electricity markets. Stochastic simulations conducted to capture uncertainty.	Matlab	[13]
Concentrated solar power (CSP)-biomass hybrid power plants	Stochastic techno-economic assessment of CSP-biomass hybrid plants. Design variables, equations, and valuation parameters provided. 33% probability of profitability, high biomass share increases profitability, add-in tariff needed for grid parity.	Matlab	[14]
Hybrid wind/solar/biomass renewable energy system with biomass power trading	Hybrid system feeds 526 million kWh/year, wind contributes 57%, biomass supplies 25% of electricity. Unmet load rate reduced to 2.92%. Operators' earnings improved compared to actual operations	Homer	[15]

Table 1. Literature review on hybrid systems with solar / biomass and/or desalination (continue).

Investigated System	Findings	Software used	Ref
Solar and biomass-based cogeneration technologies	This is a chapter that has an overview of solar and biomass-based cogeneration technologies. Discussion on efficiencies and applications in combined heat and power systems.	-	[16]
Regional energy supply combined heat and power (RES-CHP) system integrating biomass and solar energy	Development of a regional energy supply system integrating biomass and solar energy. Energy, exergy, economy, and emissions analysis conducted. Energy efficiency of 42.57%, exergy efficiency of 39.52%, CO_2 emissions of 4.146 kt/year (32.3% reduction).	Aspen Plus	[17]
Hybrid solar-biomass system for space heating and hot water supply	Optimal configuration with evacuated tube collectors: solar fraction of 57%, payback period of 4.9 years, LCOH of \$0.0642/kWh, payback period 4.9 years, annual CO_2 avoidance of 656 tons.	TRNSYS	[18]
Multi-generation hybrid biomass-solar system for providing heating, cooling, electricity, fresh-water, and hydrogen	Reduction in biomass consumption and CO2 emissions. Sensitivity analysis indicates improvement in exergy efficiency and cost rate with increased solar radiation and biomass flow rate.	Matlab	[19]
Hybrid system based on wind, hydro, solar, and biomass sources for decarbonizing the energy sector	Wind and solar complement each other, hydro shows important variability. In 2018, Romania's energy mix relied significantly on hydropower (29%), with wind and solar varying seasonally but contributing consistently to meeting EU renewable energy goals (22% share), reducing CO_2 emissions by 42%.	Homer	[20]
Solar-biomass on-grid hybrid system for Hattar Industrial Zone Phase (VII), Pakistan	Optimal configuration: 70,000 kW solar PV, 7000 kW biogas generator connected to the grid. Lowest COE of \$0.092/kWh. Payback period: 4.6 years. Reduction of 75% in carbon dioxide (CO2), 75% in sulfur oxide (SOx), and 75% in nitrogen oxide (NOx) emissions.	RET Screen	[21]
Standalone solar-wind-biomass-fuel cell energy system for rural community in Nigeria	LF-SSA algorithm optimization achieved lowest LCOE of \$0.933162/kWh and substantial cost savings compared to other algorithms and HOMER software. EMS facilitated environmentally friendly and cost-effective energy system.	Homer	[22]
Hybrid solar-biomass system for multi-family residential building	Advanced control reduces winter operation costs by 35%, applied in a residential building in Madrid. No significant reduction in summer costs.	Matlab	[23]
Biomass-solar hybrid gasification system for sustainable fuel production	Total energy conversion efficiency of 73.06%, carbon efficiency of 66.81%. Integration of solid–oxide electrolysis cells reduce electricity consumption during electrolysis by 19.30%.	Aspen Plus	[24]
Hybrid solar- and biomass-based energy system for electricity, freshwater, and hydrogen production	Proposal of an integrated system for renewable energy penetration, peak load flattening, and greenhouse gas reduction. Thermodynamic, exergo-economic, and environmental assessment conducted.	EES (Engineering Equation Solver)	[25]
Hybrid solar-biomass polygeneration system for power, heating, drying, oxygen, and ammonia production	Net power generation of 163 MW, heating of 150 MW, drying of 100 MW, oxygen production of 21.7 kmol/hr, and ammonia production of 23.24 kg/hr. Exergy efficiency: 70.68%, LCC: \$ 1.175×109, CO_2 emissions: 381.3 kg/MWh. Optimized exergy efficiency: 51.02%, LCC: 1.16×109 \$, CO_2 emissions: 359.73 kg/MWh.	Matlab	[26]
Residential building energy supply systems combining torrefied biomass gasification and solar energy	Proposal of a hybrid energy system driven by torrefied biomass gasification and solar energy. Economic analysis shows positive NPV and energy-saving benefits. Annual income of \$72,735 with 2.89 years investment recovery; reduces CO2 emissions by 550.59 tons.	RET Screen	[27]

References

[1] D. R. Santos, E. C. M. Vieira, J. T. Rocha, Q. H. S. Eugenio, and C. M. Campos, "Challenges and solutions for renewable energy storage," *Brazil. J. Prod. Eng*., vol. 9, no. 4, pp. 76–88, Oct. 2023, doi: 10.47456/bjpe.v9i4.42343.

[2] M. Farghali et al., "Social, environmental, and economic consequences of integrating renewable energies in the electricity sector: a review," *Environ. Chem. Lett*., vol. 21, pp. 1381–1418, Mar. 2023, doi: 10.1007/s10311-023-01587-1.

[3] A. Panda et al., "Recent advances in the integration of renewable energy sources and storage facilities with hybrid power systems," *Clean Eng. Tech.,* vol. 12, Feb. 2023, Art. no. 100598, doi: 10.1016/j.clet.2023.100598.

[4] A. Dağdeviren et al., "Effect of Al_2O_3-SiO_2/water hybrid nanofluid filled in a square enclosure on the natural convective heat transfer characteristics: A numerical study," *J. Nanofluids*, vol. 11, pp. 772–781, Aug. 2022, doi: 10.1166/jon.2022.1881.

[5] E. Gürsoy et al., "Energy analysis of magnetite nanofluid flowing in newly designed sudden expansion tube retrofitted with dimpled fin," *Int. J. Heat Mass Transfer*, vol. 199, Dec. 2022, Art. no. 123446, doi: 10.1016/j.ijheatmasstransfer.2022.123446.

[6] E. Gürsoy et al., "Experimental and numerical study on ferrohydrodynamic and magneto-convection of Fe_3O_4/water ferrofluid in a sudden expansion tube with dimpled fins," *J. Taiwan Inst. Chem. Eng.*, vol. 164, Nov. 2024, Art. no. 105676, doi: 10.1016/j.jtice.2024.105676.

[7] E. Gürsoy et al., "Investigation of magneto-convection characteristics in a sudden expanding channel with convex surface geometry under thermally developing flow conditions," *Int. J. Numer. Meth. Heat Fluid Flow*, vol. 34, no. 5, pp. 1969–1994, May 2024, doi: 10.1108/HFF-11-2023-0703.

[8] A. R. Jensen et al., "Demonstration of a concentrated solar power and biomass plant for combined heat and power," *Energy Convers. Manag*., vol. 271, Nov. 2022, Art. no. 116207, doi: 10.1016/j.enconman.2022.116207.

[9] H. Kaur, S. Gupta, and A. Dhingra, "Analysis of hybrid solar biomass power plant for generation of electric power," *Mater. Today: Proc*, vol. 48, no. 5, pp. 1134–1140, 2022, doi: 10.1016/j.matpr.2021.08.080.

[10] R. J. Macías et al., "Evaluation of the performance of a solar photovoltaic-biomass gasifier system as electricity supplier," *Energy*, vol. 260, Dec. 2022, Art. no. 125046, doi: 10.1016/j.energy.2022.125046.

[11] E. Aykut, B. Dursun, and S. Görgülü, "Comprehensive environmental and techno-economic feasibility assessment of biomass-solar on-grid hybrid power generation system for Burdur Mehmet Akif Ersoy University Istiklal Campus," *Heliyon*, vol. 9, no. 11, Nov. 2023, doi: 10.1016/j.heliyon.2023.e22264.

[12] A. A. Díaz Pérez, E. K. Burin, and E. Bazzo, "Part load operation analysis of a biomass steam generator integrated with a Linear Fresnel solar field," *Energy*, vol. 282, Nov. 2023, Art. no. 128590, doi: 10.1016/j.energy.2023.128590.

[13] R. Gutiérrez-Alvarez, K. Guerra, and P. Haro, "Market profitability of CSP-biomass hybrid power plants: towards a firm supply of renewable energy," *App. Energy*, vol. 335, Apr. 2023, Art. no. 120754, doi: 10.1016/j.apenergy.2023.120754.

[14] R. Gutiérrez-Alvarez, K. Guerra, and P. Haro, "Profitability of Concentrated Solar-Biomass hybrid power plants: Dataset of the stochastic techno-economic assessment," *Data in Brief*, vol. 48, Jun. 2023, Art. no. 109096, doi: 10.1016/j.dib.2023.109096.

[15] Y. Huang, Q. Wang, and J. Xu, "A stackelberg-based biomass power trading game framework in hybrid-wind/solar/biomass system: From technological, economic, environmental and social perspectives," *J. Clean. Prod*., vol. 403, Jun. 2023, Art. no. 136806, doi: 10.1016/j.jclepro.2023.136806.

[16] A. N. Srivastava, A. Kaviti, S. Chakma, and V. S. Sikarwar, "Solar and Biomass-Based Cogeneration Technologies," *Encycl. Renew. En. Sustain. Environ.*, vol. 4, pp. 263-272, 2024, doi: 10.1016/B978-0-323-93940-9.00036-0.

[17] Z. Li, X. Zhu, X. Huang, Y. Tian, and B. Huang, "Sustainability design and analysis of a regional energy supply CHP system by integrating biomass and solar energy," *Sustain. Prod. Consum*., vol. 41, pp. 228-241, Oct. 2023, doi: 10.1016/j.spc.2023.08.011.

[18] M. Krarouch, A. Allouhi, H. Hamdi, and A. Outzourhit, "Energy, exergy, environment and techno-economic analysis of hybrid solar-biomass systems for space heating and hot water supply: Case study of a Hammam building," *Renew. Energy*, vol. 222, Feb. 2024, Art. no. 119941, doi: 10.1016/j.renene.2024.119941.

[19] M. Korpeh, P. Asadbagi, A. Lotfollahi, A. Ghaemi, and A. A-Moghaddam, "4E analysis and optimization of a novel hybrid biomass-solar system: Focusing on peak load management and environmental emissions," *Process Saf. Environ. Prot.*, vol. 181, pp. 452-468, Jan. 2024, doi: 10.1016/j.psep.2023.11.035.

[20] P. Spiru, "Assessment of renewable energy generated by a hybrid system based on wind, hydro, solar, and biomass sources for decarbonizing the energy sector and achieving a sustainable energy transition," *Energy Reports*, vol. 9, no. 8, pp. 167-174, Sep. 2023, doi: 10.1016/j.egyr.2023.04.316.

[21] A. Zahid, M.K. Shahzad, S.R. Jamil, and N. Iqbal, "Futuristic feasibility analysis and modelling of a solar-biomass on-grid hybrid system for Hattar Industrial Estate Phase (VII), Pakistan," *Cleaner Energy Systems*, vol. 4, Apr. 2023, Art. no. 100053, doi: 10.1016/j.cles.2023.100053.

[22] B. Modu, Md. P. Abdullah, A. L. Bukar, M. F. Hamza, and M. S. Adewolu, "Operational strategy and capacity optimization of standalone solar-wind-biomass-fuel cell energy system using hybrid LF-SSA algorithms," *Intern. J. Hydr. Energy*, vol. 50(B), pp. 92-106, Jan. 2024, doi: 10.1016/j.ijhydene.2023.07.215.

[23] G. Zsembinszki, C. Fernández, E. Borri, and L. F. Cabeza, "Application of deep learning techniques to minimize the cost of operation of a hybrid solar-biomass system in a multi-family building," *En. Conv. Manag*., vol. 288, Jul. 2023, Art. no. 117152, doi: 10.1016/j.enconman.2023.117152.

[24] Y. Xin, X. Xing, X. Li, and H. Hong, "A biomass–solar hybrid gasification system by solar pyrolysis and PV-Solid oxide electrolysis cell for sustainable fuel production," *App. Energy*, vol. 356, Feb. 2024, Art. no. 22419, doi: 10.1016/j.apenergy.2023.122419.

[25] T. Hai, F. M. Alhomayani, P. Ghodratallah, B. S. Chauhan, H. Rajab, S. F. Almojil, A. I. Almohana, and U. Mirzat, "Proposal and ANN-assisted optimization of a hybrid solar- and biomass-based energy system for electricity, freshwater, and hydrogen production" *Int. J. Hydr. Energy*, early access, Feb. 2024, doi: 10.1016/j.ijhydene. 2024.02.126.

[26] A. Nouri, A. Chitsaz, M. Khalilian, and A. Hasanzadeh, "Analysis and optimization of a sustainable hybrid solar-biomass polygeneration system for production of power, heating, drying, oxygen and ammonia," *App. Therm. Eng*., vol. 246, Jun. 2024, Art. no. 122867, doi: 10.1016/j.applthermaleng.2024.122867.

[27] Y. Liu, D. Bi, M. Yin, K. Zhang, H. Liu, and S. Liu, "Modeling and exergy-economy analysis of residential building energy supply systems combining torrefied biomass gasification and solar energy," *Therm. Sci. Eng. Prog*., vol. 50, May 2024, Art. no. 102584, doi: 10.1016/j.tsep.2024.102584.

[28] H. Xu, S. Jiang, M. X. Xie, T. Jia, and Y. J. Dai "Technical improvements and perspectives on humidification-dehumidification desalination - a review," *Desalin*., vol. 541, Nov. 2022, Art. no. 116029, doi: 10.1016/j.desal.2022.116029.

[29] C. Fritzmann, J. Löwenberg, T. Wintgens, T. Melin, "State-of-the-art of reverse osmosis desalination," *Desalin*., vol. 216, no. 1–3, pp. 1-76, Oct. 2007. doi: 10.1016/j.desal.2006.12.009.

[30] A. P. Nicolás, A. Molina-García, J. T. García-Bermejo, and F. Vera-García, "Desalination, minimal and zero liquid discharge powered by renewable energy sources: Current status and future perspectives," *Renew. Sustain. En. Reviews*, vol. 187, Nov. 2023, Art. no. 113733, doi: 10.1016/j.rser.2023.113733.

[31] A. Yadav, P. K. Labhasetwar, and V. K. Shahi, "Membrane distillation using low-grade energy for desalination: A review," *J. Env. Chem. Eng*., vol. 9, no. 5, Oct. 2021, Art. no. 105818, doi: 10.1016/j.jece.2021.105818.

[32] M. Sedighi, M. M. B. Usefi, A. F. Ismail, and M. Ghasemi, "Environmental sustainability and ions removal through electrodialysis desalination: Operating conditions and process

parameters," *Desalination*, vol. 549, Mar. 2023, Art. no. 116319, doi: 10.1016/j.desal.2022.116319.

[33] M. M. Rashidi, I. Mahariq, N. Murshid, S. Wongwises, O. Mahian, M. A. Nazari, "Applying wind energy as a clean source for reverse osmosis desalination: A comprehensive review," *Alex. Eng. J.*, vol. 61, no. 12, pp. 12977-12989, Dec. 2022, doi: 10.1016/j.aej.2022.06.056.

[34] K. Wang, and J. W. Tester, "Sustainable management of unavoidable biomass wastes," *Green. En. Res.*, vol. 1, no. 1, Mar. 2023, Art. no. 100005, doi: 10.1016/j.gerr.2023.100005.

[35] F. A. M. Lino, K. A. R. Ismail, and J. A. Castañeda-Ayarza, "Municipal solid waste treatment in Brazil: A comprehensive review," *Energy Nexus*, vol. 11, Sep. 2023, Art. no. 100232, doi: 10.1016/j.nexus.2023.100232.

[36] S. Vyas, P. Prajapati, A. V. Shah, V. K. Srivastava, and S. Varjani, "Opportunities and knowledge gaps in biochemical interventions for mining of resources from solid waste: A special focus on anaerobic digestion," *Fuel*, vol. 311, Mar. 2022, Art. no. 122625, doi: 10.1016/J.FUEL.2021.122625.

[37] A. Khosravi, S. Santasalo-Aarnio, and S. Syri, "Optimal technology for a hybrid biomass/solar system for electricity generation and desalination in Brazil," *Energy*, vol. 234, Nov. 2021, Art. no. 121309, doi: 10.1016/j.energy.2021.121309.

[38] E. B. Pereira et al., *Brazilian Atlas of Solar Energy*, 2nd ed., São José dos Campos, Brazil: INPE, 2017, p. 80, doi: 10.34024/978851700089.

[39] Labren, "Brasil-SR Model," Accessed: Aug. 5, 2024. [Online]. Available: https://labren.ccst.inpe.br/brasil-sr.html

[40] ABREMA, "Panorama of Solid Waste in Brazil," Accessed: Oct. 5, 2024. [Online]. Available: https://abrelpe.org.br/panorama/

[41] A. Calbry-Muzyka, H. Madi, F. Rüsch-Pfund, M. Gandiglio, and S. Biollaz, "Biogas composition from agricultural sources and organic fraction of municipal solid waste," *Renew. Energy*, vol. 181, pp. 1000-1007, Jan. 2022, doi: 10.1016/j.renene.2021.09.100.

[42] A. Kumar, and S. R. Samadder, "Development of lower heating value prediction models and estimation of energy recovery potential of municipal solid waste and RDF incineration," *Energy*, vol. 274, Jul. 2023, Art. no. 127273, doi: 10.1016/j.energy.2023.127273.

[43] M. Ioelovich, "Energy Potential of Natural, Synthetic Polymers and Waste Materials - A Review," *Academ. J. Polym. Sci.*, vol. 1, no. 1, May 2018 doi: 10.19080/AJOP.2018.01.555553.

[44] C. Bispo, C. Colombo, R. Braz, M. Medeiros, and F. Souza, "Selective collection in Natal/RN: scenario of recyclable materials cooperatives," *Metrop. J. Sustain.*, vol. 7, no. 1, pp. 141-160, Jan./Apr. 2017, (in Portuguese).

[45] G. O. Santos, and F. B. S. Mota, "Gravimetric composition of household solid waste in Fortaleza - CE disposed at the Caucaia/CE landfill," *Technol. J.*, vol. 31, no. 1, pp. 39-50, (in Portuguese), Jun 2010.

[46] G. P. Narayan, K. H. Mistry, M. H. Sharqawy, S. M. Zubair, and J. H. Lienhard, "Energy effectiveness of simultaneous heat and mass exchange devices," *Front. Heat and Mass Trans.*, vol. 1, no. 2, pp. 1-13, Jul. 2010, doi: 10.5098/hmt.v1.2.3001.

[47] M. H. Sharqawy, J. H. Lienhard, and S. M. Zubai, "Thermophysical properties of seawater: A review of existing correlations and data," *Desalin. and Water Treat.*, vol. 16, no. 1-3, pp. 354-380, Aug. 2012, doi:10.5004/dwt.2010.1079.

[48] L. Pagnini, S. Bracco, F. Delfino, and M. Simón-Martin, "Levelized cost of electricity in renewable energy communities: Uncertainty propagation analysis," *Appl. Energy*, vol. 366, Jul. 2024, Art. no. 123278, doi: 10.1016/j.apenergy.2024.123278.

[49] M. J. B. Kabeyi, and O. A. Olanrewaju, "The levelized cost of energy and modifications for use in electricity generation planning," *Energy Rep.*, vol. 9, Supp 9, pp. 495-534, Sep. 2023, doi: 10.1016/j.egyr.2023.06.036.

[50] A. H. Alami et al., "Concentrating solar power (CSP) technologies: Status and analysis," *Int. J. Thermofluids*, vol. 18, May 2023, Art. no. 100340, doi: 10.1016/j.ijft.2023.100340.

[51] M. D. Rey, R. Font, and I. Aracil, "Biogas from MSW landfill: Composition and determination of chlorine content with the AOX (adsorbable organically bound halogens) technique," *Energy*, vol. 63, pp. 161-167, Dec. 2013, doi: 10.1016/j.energy.2013.09.017.

[52] N. Dadario et al., "Waste-to-energy recovery from municipal solid waste: Global scenario and prospects of mass burning technology in Brazil," *Sustainability*, vol. 15, no. 6, Mar. 2023, Art. no. 5397, doi: 10.3390/su15065397.

[53] M. S. Riaz, K. J. Barb, and A. Engeda, "A Novel Technique for Steam Turbine Exhaust Pressure Limitation Using Dynamic Pressure Sensors," *Proc. of the Inst. of Mech. Eng., Part C: J. Mech. Eng. Sci.*, vol. 219, no. 9, pp. 925-932, Sep. 2005, doi:10.1243/095440605X31805.

[54] V. Mrzljak, T. Senčić, and B. Žarković, "Turbogenerator Steam Turbine Variation in Developed Power: Analysis of Exergy Efficiency and Exergy Destruction Change," *Modell. Simul. Eng.*, vol. 2018, no. 1, Jul. 2018, Art. no. 2945325, doi: 10.1155/2018/2945325.

[55] IPCC, Chapter 2: Stationary Combustion, in *2006 IPCC Guidelines for National Greenhouse Gas Inventories*, vol. 2: Energy. Accessed: Oct. 1, 2024. [Online]. Available: https://www.ipcc-nggip.iges.or.jp

[56] Q. Liu et al., "Thermodynamics investigation of a solar power system integrated oil and molten salt as heat transfer fluids," *App. Therm. Eng.*, vol. 93, pp. 967-977, Jan. 2016, doi: 10.1016/j.applthermaleng.2015.10.071.

[57] T. P. van der Stelt, E. Casati, N. Chan, and P. Colonna, "Technical equation of state models for heat transfer fluids made of biphenyl and diphenyl ether and their mixtures," *Fluid Phase Equilibria*, vol. 393, pp. 64-77, May 2015, doi: 10.1016/j.fluid.2015.02.025.

[58] V-E. Cenuşă et al., "Energetic and exergetic analysis of Rankine cycles for solar power plants with parabolic trough and thermal storage," *Renew. Energy Environ. Sustain.*, vol. 1, May 2016, doi: 10.1051/rees/2016010.

[59] Eastman, "Therminol VP-1 Technical Bulletin 7239115B," Accessed: June 3, 2024. [Online]. Available: https://www.therminol.com/sites/therminol/files/documents/TF09A_Therminol_VP1.pdf